



# CHAOTIC DIFFUSION IN MULTIDIMENSIONAL CONSERVATIVE MAPS

PABLO M. CINCOTTA\* and CLAUDIA M. GIORDANO†

*Grupo de Caos en Sistemas Hamiltonianos,  
Facultad de Ciencias Astronómicas y Geofísicas,  
Universidad Nacional de La Plata, and  
Instituto de Astrofísica de La Plata (CONICET)  
Paseo del Bosque, B1900FWA La Plata, Argentina*

*\*pmc@fcaglp.unlp.edu.ar  
†giordano@fcaglp.unlp.edu.ar*

Received February 9, 2011; Revised August 3, 2011

In the present paper, we provide results and discussions concerning the processes that lead to local and global chaotic diffusion in the phase space of multidimensional conservative systems. We investigate and provide a measure of the extent of the domain over which diffusion may occur. All these issues are thoroughly discussed by dealing with a multidimensional conservative map that would be representative of the dynamics of a resonance interaction, which is an important mechanism in many dynamical systems.

*Keywords:* Chaos; diffusion; instabilities; resonance interaction.

## 1. Introduction

One of the lesser known processes in multidimensional Hamiltonian systems is the so-called *chaotic diffusion*, that is, those mechanisms under which either global or local actions of an integrable Hamiltonian change over phase space (or action space) under the effect of a nonintegrable perturbation. This kind of phenomena arises in Solar System dynamics, stellar dynamics such as star clusters and galaxies as well as in many other dynamical problems.

Up to the present day, there does not exist any theory that could describe global diffusion in phase space of multidimensional systems. One could acquire accurate values of several indicators of the stability of the motion, but they would only provide local information in a neighborhood of a given point of phase space. A given orbit in a chaotic component in a 3D potential could have, for instance, positive

and large values of two of its Lyapunov exponents, which does not necessarily mean that the unperturbed integrals will vary over vast domains.

Even though near-integrable Hamiltonian systems have been largely investigated — perhaps starting with the study conducted by Poincaré in the late nineteenth century [Poincaré, 1893] — the problem has not been completely elucidated yet. In fact, questions such as the stability of the motion of high-dimensional systems are far from being thoroughly understood. Some progress on transport phenomena has been made during the last two decades (see e.g. [Meiss, 1992; Venegeroles, 2008]), but almost all the attained results concern only low-dimensional symplectic maps or in other cases, nonconservative one-dimensional maps (see e.g. [Korabel & Klages, 2004]), and it appears rather difficult to extend these approaches to apply to many-dimensional Hamiltonians or conservative

maps. Moreover, it is unclear how these approaches provide information about the role played by the torus structure and their invariant manifolds in spreading or preventing diffusion in phase space.

Developing further in this direction, Chirikov [1979] pioneered a complete survey of this matter in a somewhat heuristic way by using a standard mathematical language. Following this improvement, Cincotta [2002], revisited Chirikov's arguments, particularly that related to the so-called Arnol'd diffusion.

Regarded as a global instability, Arnol'd diffusion appears to be closer to a theoretical conjecture rather than to a real physical process (see [Arnol'd, 1964; Chirikov & Vecheslavov, 1989, 1993; Chirikov *et al.*, 1984; Cincotta, 2002]). In fact, there remain so many unsolved mathematical details that Arnol'd diffusion, as a global instability, results in a rather controversial question (see [Lochak, 1999]). Further, the more recent numerical evidence reveals that Arnol'd diffusion might operate in certain (somewhat artificial) dynamical systems.

Nonetheless, it has been shown that Arnol'd diffusion-like processes may play a significant role in global chaotic diffusion in phase space [Giordano & Cincotta, 2004; Cachucho *et al.*, 2010], though the mechanisms that drive the diffusion remain still unknown.

In [Cachucho *et al.*, 2010] Chirikov's diffusion approach is applied to the  $(5, -2, -2)$  three-body mean motion resonance for the (490) Verita's family. It is shown that the theoretical arguments used by Chirikov to describe Arnol'd diffusion could also apply in this realistic problem in which the so-called guiding resonance domain is completely chaotic. However, the scenario of modulational diffusion [Chirikov *et al.*, 1984] could perhaps be more suitable to describe the large diffusion observed in the eccentricity of asteroids.

On the other hand, in [Giordano & Cincotta, 2004] the authors presented a preliminary study of diffusion on phase space for a rather simple dynamical system in order to elucidate its efficiency to connect different chaotic components. Despite the simplicity of the adopted model, several results concerning its dynamics can be applied to any 3D Hamiltonian system exhibiting a divided phase space, such as galactic or planetary systems. Two values for the perturbation parameter have been selected so that the dynamics of the toy model resembles that of a galactic system (for a

moderate perturbation, in which case both components are comparable) and asteroidal dynamics (for a large perturbation for which the chaotic component prevails).

In this direction, Giordano and Cincotta [2004] showed that diffusion might actually take place over the full chaotic component only for strong chaotic dynamics, where resonances are almost all destroyed by overlap, and for very large time-scales. Notice that while time-scales of the order of  $\sim 6 \times 10^8$  characteristic periods are physically significant in, for instance, asteroidal dynamics, they are completely irrelevant for galactic systems, for which  $\sim 10^3$  periods is an upper bound for realistic time-scales. Anyway, despite the motion time elapsed in the case of moderate perturbations, diffusion seems unable to connect different stochastic domains.

Observational evidence, theoretical arguments and N-body simulations suggest that a model resembling an isolated elliptical galaxy should exhibit a divided phase space and therefore the perturbation should be moderate (see, e.g. [Merritt & Friedman, 1996; Merritt & Valluri, 1996; Papaphilippou & Laskar, 1998; Gerhard & Binney, 1985; Poon & Merritt, 2002; Muzzio *et al.*, 2005]).

In that case, we have observed that the unperturbed integrals remain confined to rather small chaotic domains and diffusion is completely unable to connect different chaotic domains, at least over time-scales of the order of  $\sim 10^8$  characteristic periods, several orders of magnitude larger than the typical time-scales for galactic systems.

In the present effort we show, discuss and measure chaotic diffusion in action space by means of a conservative multidimensional map, the Coupled Rational Shifted Standard Map (CRSSM), whose global dynamical properties have been previously studied in [Cincotta & Giordano, 2008; Cincotta *et al.*, 2003], CGS03 hereafter, for different sets of parameters, by recourse of the Mean Exponential Growth Factor of Nearby Orbits (MEGNO). First introduced by Cincotta and Simó [2000] and later generalized in CGS03, the MEGNO is a rather efficient indicator of the dynamics belonging to the class of the so-called fast indicators, which is already of widespread use. Many applications of this tool to Solar System dynamics, exoplanets models and as well as to many other dynamical systems could be found throughout the literature.

Having attained the global dynamical picture of the system under consideration, we investigate chaotic diffusion in locally strongly unstable regions. We show that what is called Arnol'd diffusion-like processes only take place when the relics of resonances are strongly unstable (hyperbolic). We also yield numerical evidence that even in the case of a largely chaotic phase space, diffusion becomes almost irrelevant, which is referred to as stable chaos. Several papers due to Milani and co-workers [Milani & Nobili, 1992; Milani, 1993; Milani & Farinella, 1994; Milani *et al.*, 1997] also address this topic. Moreover, further studies deal with the same phenomena of stable chaos [Morbidelli & Froeschlé, 1996], which arises, for instance, in Solar System dynamics.

Furthermore, we provide a simple tool which appears to be suitable for measuring the variation of the unperturbed integrals.

Herein we face the difficulty to compute a meaningful diffusion coefficient, due to the fact that, as far as we know, it still remains unclear which would be the appropriate approach to be considered, in particular, how the variance of the variables scales with time. In fact, in the case of normal diffusion the variance scales linearly with time, but for what is called abnormal diffusion, the scaling runs like  $t^b$  where the parameter  $b$  is, in general, unknown and further, it strongly depends on the local dynamical structure of the deemed region of phase space. Some other more recent developments like the one called super-diffusion should also be mentioned.

An exhaustive numerical exploration is performed and the results of their application are discussed.

The paper is organized as follows. In Sec. 2 we provide a brief summary on the MEGNO when adapted to investigate the global dynamics in multidimensional discrete dynamical systems. Section 3 is devoted to describe the 4D map used in this research, namely, the Coupled Rational Shifted Standard Map (CRSSM), that models the interaction of two resonances. Its dynamical properties as well as a picture of the structure of its phase space unveiled by recourse to the MEGNO are described in Sec. 6, while with the aim of measuring the change of the unperturbed integrals a diffusion measure is introduced, the finite time Shannon or Arnol'd Entropy. Conclusions and final remarks are given in Sec. 7.

## 2. The Mean Exponential Growth Factor of Nearby Orbits (MEGNO) for Maps

For exploring phase space in the present effort, we wield the MEGNO, one of the so-called fast indicators of dynamics.

The main features of the MEGNO, its performance when applied to the study of global dynamics in 2D Hamiltonians as well as the advantages of deriving the largest Lyapunov Characteristic Number (LCN) from a least squares fit on the time evolution of the MEGNO can be found in CGS03 [Cincotta & Simó, 2000; Cincotta & Giordano, 2002].

The generalized version of the MEGNO, along with its implementation to discrete dynamical systems, which is in order for the current applications, are also given in CGS03. Though, just for the sake of completeness, permit us to provide a brief description of how this tool should be applied in the latter case.

For a given map  $P$ , the initial point  $Q_0$  is iterated to yield the points  $Q_k = P^k(Q_0)$ , while the differential map DP transports an initial "random" tangent vector,  $v_0$ ,  $\|v_0\| = 1$ , providing vectors  $v_k = DP^k(Q_0)v_0$ . Then, after  $N$  iterates, the generalized MEGNO is computed by means of

$$Y_{m,n}(N) = (m+1)N^n \sum_{k=1}^N \ln \left( \frac{\|v_k\|}{\|v_{k-1}\|} \right) k^m, \quad (1)$$

and

$$\bar{Y}_{m,n}(N) = \frac{1}{N^{m+n+1}} \sum_{k=1}^N Y_{m,n}(k). \quad (2)$$

As already discussed in CGS03, the larger  $m$ , the faster  $\bar{Y}_{m,n}$  converges to a constant value for regular, quasiperiodic motion, but, for  $m$  rather large, small oscillations show up, which may be attenuated by stopping the iteration when the distance between the initial and final points is minimum ("right-stop" condition).

Further, a slight additional modification becomes beneficial for the choice (2, 0) of the exponents  $(m, n)$ , which leads us to the quantity

$$\hat{Y}_{2,0}(N) = \frac{[4\bar{Y}_{2,0}(N) - 2]}{N}, \quad (3)$$

which tends to  $0^-$  in the regular case and to  $\sigma_i$ , which is the LCN of the orbit, in the case of

an irregular trajectory. Negative values of  $\hat{Y}_{2,0}(N)$  appear for regular orbits, provided  $N$  is taken not too small, while small positive values identify mild chaos.

Even when a linear fit of  $[4\bar{Y}_{2,0}(N) - 2]$  could eventually improve resolution, the plain use of (3) with the “right-stop” condition,  $\hat{Y}_{2,0,rs}$ , suffices for our goals.

### 3. On a Multidimensional Map: The Coupled Rational Shifted Standard Map (CRSSM)

Let us introduce the 4D conservative map that we undertake as subject of our experimentation, namely, the Coupled Rational Shifted Standard Map (CRSSM) which provides a fairly good representation of the interaction of two perturbed resonances. Therefore, its dynamics would well serve to model many dynamical scenarios.

The CRSSM is described by the equations

$$\begin{aligned} y'_1 &= y_1 + \epsilon_1 f_1(x_1) + \gamma_+ f_3(x_1 + x_2) \\ &\quad + \gamma_- f_3(x_1 - x_2), \\ y'_2 &= y_2 + \epsilon_2 f_2(x_2) + \gamma_+ f_3(x_1 + x_2) \\ &\quad - \gamma_- f_3(x_1 - x_2), \\ x'_1 &= x_1 + \epsilon_1 y'_1, \\ x'_2 &= x_2 + \epsilon_2 y'_2, \end{aligned} \tag{4}$$

with  $x_i \in [0, 2\pi)$ ,  $y_i \in [0, 2\pi/\epsilon_i)$ ,  $i = 1, 2$ , and

$$\begin{aligned} f_i(x) &= \frac{\sin(x + \varphi_i)}{1 - \mu_i \cos x} - \Delta_i, \\ \Delta_i &= \frac{\mu_i \sin \varphi_i}{\sqrt{1 - \mu_i^2} + 1 - \mu_i^2}, \quad i = 1, 2, 3, \end{aligned} \tag{5}$$

where  $\mu_i \in [0, 1)$ , and the quantities  $\Delta_i$  are fixed so that  $f_i$  functions have zero average.

Let us note that (4) consists of two coupled standard maps so modified that symmetry is lost through the introduction of the phase  $\varphi_i$ , and the entire character of  $f_i$  is broken due to the introduction of the parameters  $\mu_i \in [0, 1)$ . The coupling terms in  $(x_1 + x_2)$  and  $(x_1 - x_2)$  encompass the parameters  $\gamma_+$  and  $\gamma_-$ , respectively. Thus defined, the map is a four-dimensional torus.

It could be claimed that the deemed map has too many free parameters. Note however that most of them are kept fixed in all our study,  $\epsilon_2$  being the only one to be varied.

It is fair to state clearly that in this section we summarize those particular results which are pertinent to the purpose of the present work. The dynamical picture of this map for different sets of coupling parameters and  $\epsilon_i$  is addressed in CGS03.

The parameters for the model assumed as fixed are  $\mu_1 = 0.5, \varphi_1 = 1, \mu_2 = 0.4, \varphi_2 = 2, \mu_3 = 0.6, \varphi_3 = 3, \epsilon_1 = 0.1, \gamma_+ = 0.1$  and  $\gamma_- = 0.05$ . Two distinct values of  $\epsilon_2$ , one positive and the other negative, 0.2 and  $-0.2$ , were taken in order to spot the diverse effect of such a choice on the resulting dynamics.

#### 3.1. Results provided by the MEGNO

For constructing Fig. 1, the MEGNO was computed for an equi-spaced grid of  $1000 \times 1000$  pixels in the domain  $(y_1 \epsilon_1 / 2\pi, y_2 \epsilon_2 / 2\pi) \in [0, 1) \times [0, 1)$ , the initial values for the remaining variables being  $x_1 = 0, x_2 = 0$ . Recall that this is a problem of higher dimension, so that the iterates under DP of two “random” initial vectors  $v_{10}, v_{20}$ , satisfying  $\|v_{i0}\| = 1$ , had to be computed, plus orthogonalized and renormalized at each step, and the maximum of the two resulting values of  $\hat{Y}_{2,0,rs}$ , one associated to each direction, was taken to determine the character of each trajectory. The picture on the right corresponds to  $\epsilon_2 = 0.2$  and the one on the left to  $\epsilon_2 = -0.2$ .

The contour-like plots exhibit the obtained values for  $\log(\hat{Y}_{2,0,rs})$  after  $N = 10^4$  iterations, so that the details in each figure be highlighted. The initial conditions depicted in white correspond to regular orbits, while those in red are considered strongly chaotic. The intermediate range is regarded as corresponding to, possibly, mildly chaotic motion. It is interesting to remark that in the coupling we face to an indefinite form rather than a positive definite one, which produces a pretty dramatic effect on the resonances. In fact, observe that in the case of positive  $\epsilon_2$  most of the resonances have an elliptical chain of tori at their center while for the negative value of such a parameter several resonances show up as totally hyperbolic. Note that we are dealing with *a priori* unstable system (see for instance [Lega *et al.*, 2010]).

Again, for a thorough discussion we refer to CGS03, but a brief description of the outstanding features are included herein for the sake of clarity and adroitness.

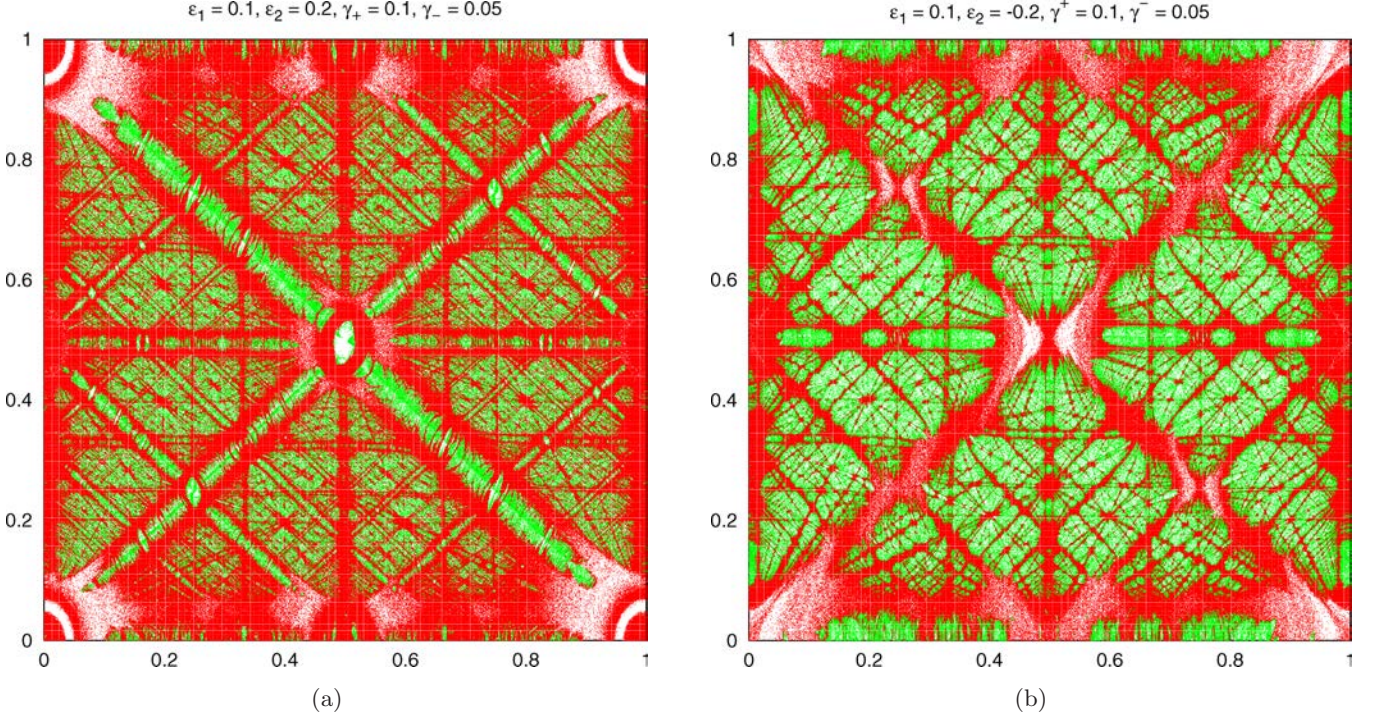


Fig. 1.  $\hat{Y}_{2,0,rs}$  levels for the CRSSM on the  $(y_1, y_2)$ -plane taking values of  $\epsilon_2$  with opposite signs (0.2 on the left and  $-0.2$  on the right). Initial conditions of regular behavior are plotted in white, those of mild local instability in green while those exhibiting strong local instability in red.

A resonance can be identified as a white or green channel surrounded by red boundaries: the elliptic center and the hyperbolic border. Alternatively, only the hyperbolic structure is observed, as a consequence of the phase shift that takes place when the sign of  $\epsilon_2$  is reversed.

The resonances in the vertical and horizontal directions are present even if  $\gamma_{\pm} = 0$  and their amplitudes depend, essentially, on  $\epsilon_j$ ,  $j = 1, 2$ . These resonances appear as white or green channels, despite the sign of  $\epsilon_2$  and are the same in the uncoupled Standard Map. Indeed, the sign of  $\epsilon_i$  does not modify the uncoupled map, but it certainly affects the coupled one, since rescaling the  $y$ -variables, the CRSSM can be recast as

$$\begin{aligned}
 y'_1 &= y_1 + \epsilon_1^2 f_1(x_1) + \epsilon_1 \gamma_+ f_3(x_1 + x_2) \\
 &\quad + \epsilon_1 \gamma_- f_3(x_1 - x_2), \\
 y'_2 &= y_2 + \epsilon_2^2 f_2(x_2) + \epsilon_2 \gamma_+ f_3(x_1 + x_2) \\
 &\quad - \epsilon_2 \gamma_- f_3(x_1 - x_2), \\
 x'_1 &= x_1 + y'_1, \\
 x'_2 &= x_2 + y'_2,
 \end{aligned} \tag{6}$$

where  $(x_i, y_i) \in [0, 2\pi) \times [0, 2\pi)$ .

As long as the coupling parameters are increased, resonances become wider and several new resonances arise, namely, those of the form  $\alpha y_1 + \beta y_2 = \text{const}$ , with  $\alpha$  and  $\beta$  nonvanishing constants. In fact, the map (6) can be derived from the 2.5 degrees of freedom Hamiltonian

$$\begin{aligned}
 H(p_1, p_2, x_1, x_2, t; \epsilon_1, \epsilon_2) \\
 &= H_0(p_1, p_2, x_1, x_2, t; \epsilon_1, \epsilon_2) \\
 &\quad + \gamma_+ V_p(x_1, x_2, t; \epsilon_1, \epsilon_2) \\
 &\quad + \gamma_- V_n(x_1, x_2, t; \epsilon_1, \epsilon_2),
 \end{aligned} \tag{7}$$

where

$$\begin{aligned}
 H_0(p_1, p_2, x_1, x_2, t; \epsilon_1, \epsilon_2) \\
 &= \frac{(p_1^2 + p_2^2)}{2} + (\epsilon_1^2 U_1(x_1) + \epsilon_2^2 U_2(x_2)) \delta_{2\pi}(t), \\
 p_i &= \frac{y_i}{2\pi}, \quad f_i(x_i) = -\frac{1}{2\pi} \frac{dU_i}{dx_i}, \quad i = 1, 2,
 \end{aligned} \tag{8}$$

$\delta_{2\pi}(t)$  being the  $2\pi$ -periodic delta defined through its Fourier expansion so that  $t \bmod(2\pi)$ , and the

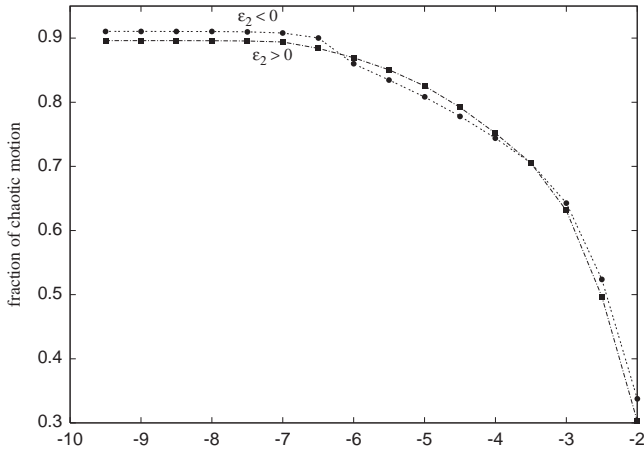


Fig. 2. Fraction of chaotic motion in the maps corresponding to  $\epsilon_2 = 0.2$  and  $\epsilon_2 = -0.2$  against different threshold values of  $\log(\hat{Y}_{2,0,rs})$ .

coupling terms can be written as

$$\begin{aligned} V_p(x_1, x_2, t; \epsilon_1, \epsilon_2) &= (\epsilon_1 + \epsilon_2)U_3(x_1 + x_2)\delta_{2\pi}(t), \\ V_n(x_1, x_2, t; \epsilon_1, \epsilon_2) &= (\epsilon_1 - \epsilon_2)U_3(x_1 - x_2)\delta_{2\pi}(t). \end{aligned} \tag{9}$$

The relationship between  $f_3$  and  $U_3$  is similar to that defined above involving  $f_i$  and  $U_i$  for  $i = 1, 2$ . Since all functions of  $t, x_1, x_2$  are periodic, their Fourier expansion generates all kind of resonances that, in action space, appear as straight lines. Indeed, the unperturbed frequencies, that is when  $\epsilon_i = \gamma_i = 0$ , are  $(\omega_1, \omega_2) = (y_1, y_2)$ .

Let us now refer to Fig. 2 which displays the fraction of chaotic motion for the maps corresponding to the two opposite values of  $\epsilon_2$ , for different thresholds of  $\log(\hat{Y}_{2,0,rs})$  below which the global motion is regarded as regular. From this figure it could be deduced that  $\log(\hat{Y}_{2,0,rs}) \approx -6.5$  is a fairly adequate value to be adopted as a threshold in order to separate regular from chaotic dynamics. Notice that, for both values of  $\epsilon_2$ , action space is almost completely chaotic, only about 10% corresponding to regular motion, so it can be claimed that global chaos was set up in the system.

These results could be misleading since one might erroneously expect the behavior of the multidimensional map (4) to have similar dynamical properties for both values of  $\epsilon_2$ , which is certainly not the case as we show in the forthcoming section.

#### 4. Diffusion on Action Space

With the aim of gaining some insight on the way diffusion operates, and to illustrate it, several orbits

with initial conditions embedded in different chaotic domains were traced onto action space for both values of  $\epsilon_2$ .

The wandering of the unperturbed integrals on the  $(y_1, y_2)$ -plane was pursued during  $10^7$  iterations for the initial conditions listed in Table 1, which are not only located near the crossing of resonances, but in the most, have high values of the MEGNO (exceptions are the initial conditions (iv) for  $\epsilon_2 = 0.2$  and (i) for  $\epsilon_2 = -0.2$ , since they correspond to stable motion).

As shown in Fig. 3(a) (corresponding to  $\epsilon_2 = 0.2$ ), the unperturbed integrals remain confined to rather small domains, so that diffusion turns out to be inefficient for a rather large number of iterates.

On the other hand, the plot in Fig. 3(b), corresponding to  $\epsilon_2 = -0.2$ , exhibits the significant efficacy of the diffusive process (except for the initial condition (i) defining a stable orbit), and evinces that the relics of the unperturbed resonances serve as paths for diffusion, mechanism termed Arnol'd diffusion-like process and should not be confused with Arnol'd diffusion. A detailed discussion about this issue and its departure from actual Arnol'd diffusion could be found in [Giordano & Cincotta, 2004; Cachucho *et al.*, 2010] as well as in CGS03. Nonetheless, let us stress that the observed diffusion presents a geometrical resemblance with the Arnol'd theoretical conjecture according to which diffusion proceeds on phase space through the chaotic layers of the resonance web.

Moreover, Figs. 4(a) and 4(b) illustrate that the orbits with initial conditions (ii) and (iv) for the case of  $\epsilon_2 = -0.2$  sweep a rather large fraction of action space after  $2 \times 10^8$  iterations. Notice must be taken however that the chaotic component of phase space is not fully connected for this time-scale, since some chaotic domains remain unreachable.

Table 1. Initial conditions on action space in units of  $2\pi/\epsilon_j$ ,  $j = 1, 2$  (the same as in Fig. 1) for five different orbits and its concomitant value of  $\log(\hat{Y}_{2,0,rs})$  for  $\epsilon_2 = 0.2$  (fourth column) and  $\epsilon_2 = -0.2$  (last column) after  $10^4$  iterations.

| i.c.  | $y_1$ | $y_2$ | $\log(\hat{Y}_{2,0,rs})$<br>$\epsilon_2 = 0.2$ | $\log(\hat{Y}_{2,0,rs})$<br>$\epsilon_2 = -0.2$ |
|-------|-------|-------|--|---|
| (i)   | 0.000 | 0.110 | -2.435   | -10.000   |
| (ii)  | 0.000 | 0.500 | -1.584   | -1.436  |
| (iii) | 0.331 | 0.353 | -1.712   | -1.486  |
| (iv)  | 0.500 | 0.500 | -10.000  | -1.449  |
| (v)   | 0.074 | 0.336 | -1.824   | -1.794  |

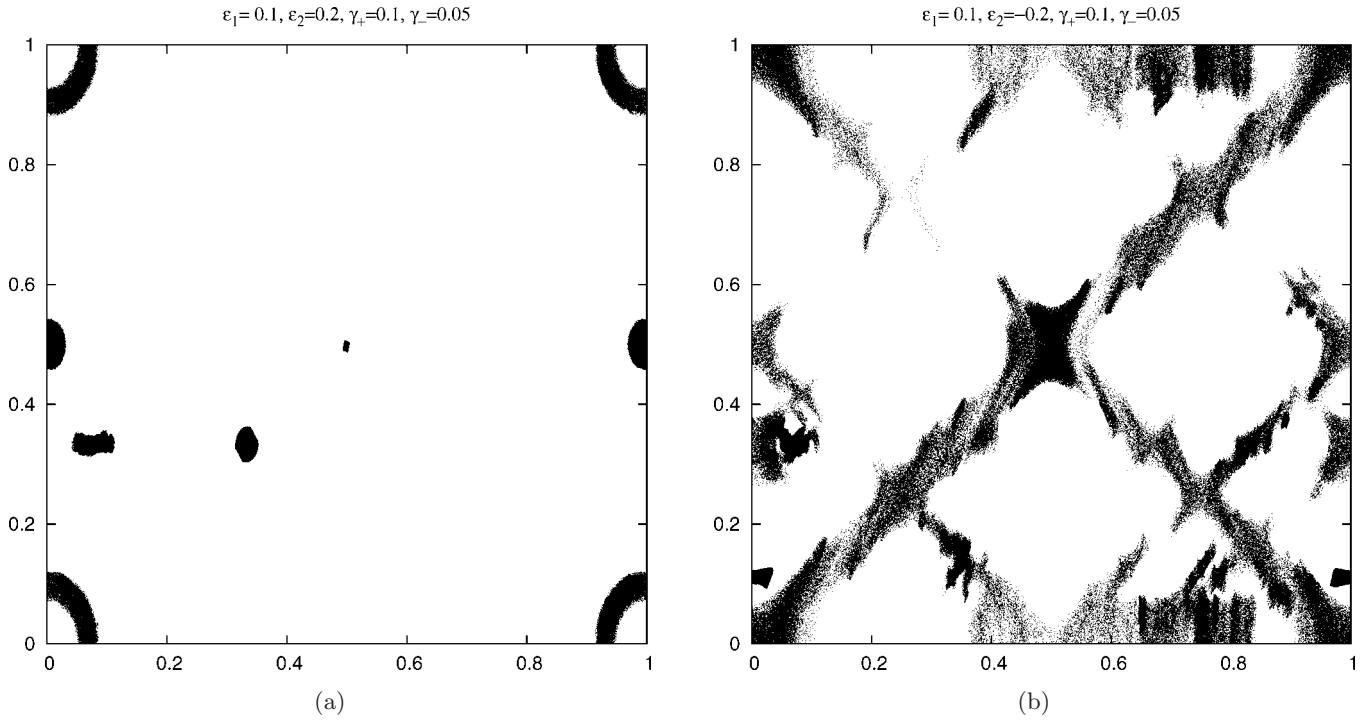


Fig. 3. Diffusion on action space after  $10^7$  iterations of the map for the initial conditions listed in Table 1.

Figure 5 depicts the time evolution of the initial condition (iv) after  $10^9$  (in red) and  $2 \times 10^9$  (in green) iterations of the map for  $\epsilon = -0.2$ . Even during the last  $10^9$  iterates when the orbit explores

some additional resonance remnants, it is still far from visiting the entire chaotic component [compare with Fig. 1(b)]. Furthermore, since the trajectory seems to remain trapped in the horizontal resonance

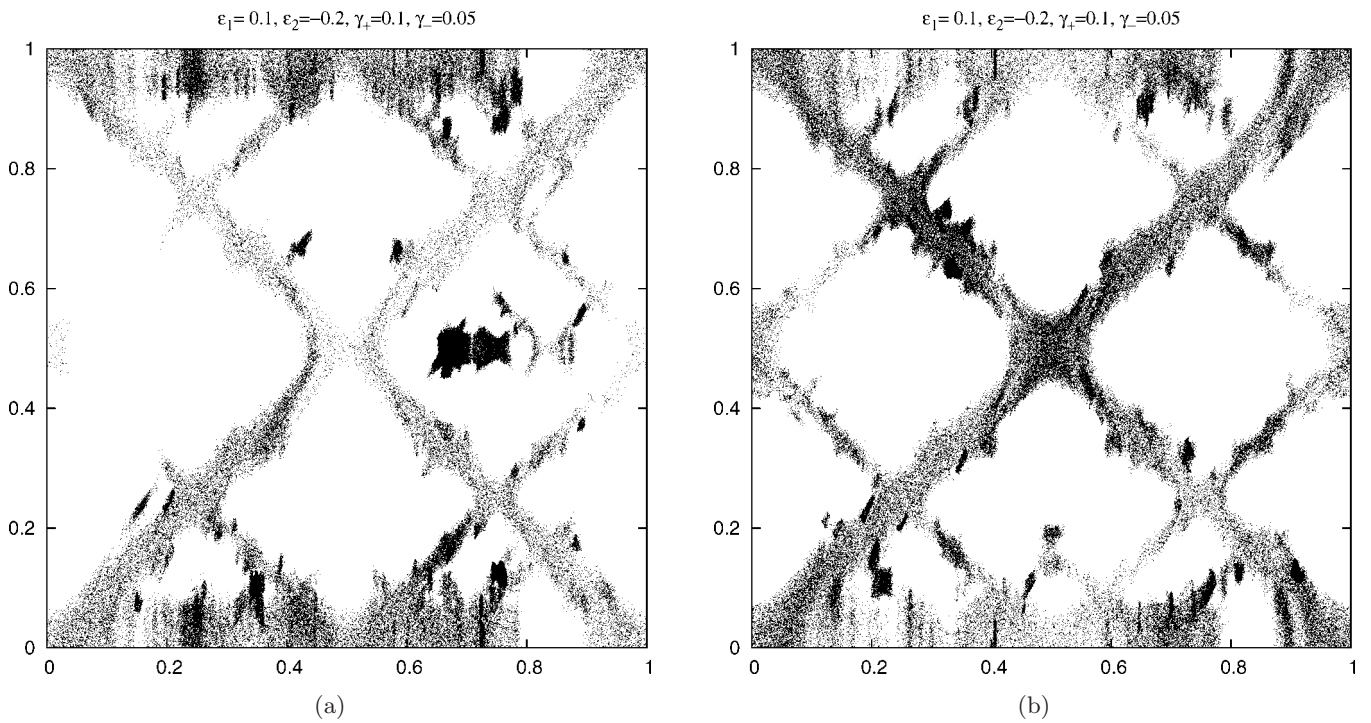


Fig. 4. Diffusion on action space after  $2 \times 10^8$  iterations of the map corresponding to  $\epsilon_2 = -0.2$  for (a) i.c. (ii) and (b) i.c. (iv).

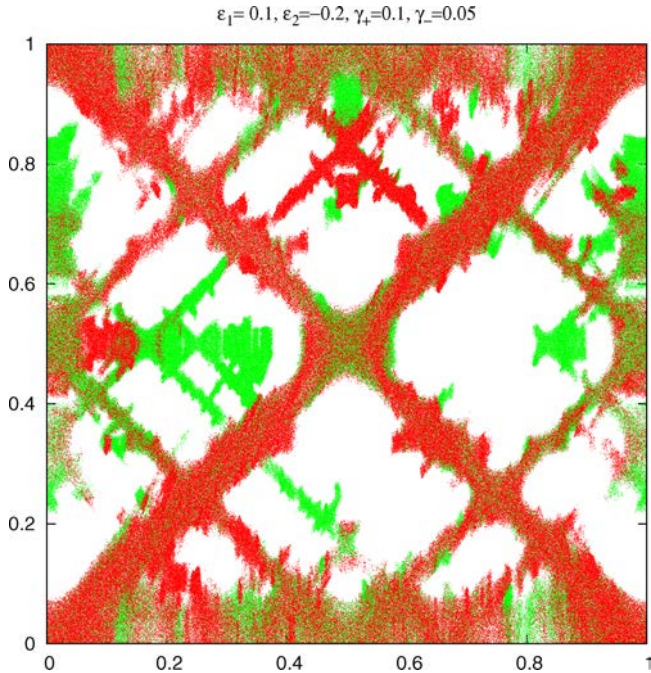


Fig. 5. Diffusion on action space corresponding to  $\epsilon = -0.2$  for i.c. (iv) after  $10^9$  iterates (red), and after  $2 \times 10^9$  (green).

at  $y_2 = 0.5$  (which has an elliptic structure), no significant difference between the domains swept in the two lapses of time is observed.

Indeed, these plots could be considered as a time-contour diagram, since the more crowded regions should be associated to those domains of action space where the orbit spends more time. Maybe in the limit, when  $N \rightarrow \infty$ , a single orbit embedded in a chaotic domain would contrive to cover the whole chaotic component, but in a finite lapse of time this seems not to be the case.

## 5. A Measure of Diffusion

The usual approach for studying diffusive processes associated with the variation of a certain quantity involves the analysis of the evolution of its mean square displacement. Certainly, the type of diffusion most studied is the normal diffusion, mainly characterized by the linear scaling of the mean square displacement with time. Though, deviations from normal diffusion are frequently observed in many dynamical systems (see for instance [Zhou *et al.*, 2002; Cordeiro & Mendes de Souza, 2005; Cordeiro, 2006]). This phenomena, termed anomalous diffusion in [Metzler & Klafter, 2000], affords also a characterization through the scaling of the variance with time but of a more general form.

Herein, we undergo the computation of a diffusion coefficient under the framework of normal diffusion in a rather simple fashion, following [Chirikov, 1979].

Instead of tracing the evolution of a single orbit of the map, a diffusion coefficient for an ensemble of nearby orbits could be computed. To this end, and following the standard procedure in the case of random walk processes, let us define the finite time diffusion coefficient as the mean-square spread in  $y_i$  as (see [Meiss, 1992])

$$\hat{D}_i = \frac{\text{Var}[y_i]}{N}, \quad (10)$$

where  $\text{Var}[y_i]$  stands for the variance of the action and  $N$  for the entire time or number of iterates, so that the mean square span in each unperturbed action is given by

$$\sigma_i[y_i] = \sqrt{N\hat{D}_i}. \quad (11)$$

Finally, we introduce the quantity

$$D = \frac{\hat{D}_1 + \hat{D}_2}{2} \quad (12)$$

as a measure of the normal diffusion on the unperturbed action-plane.

Recall that the map (4) is defined on a torus so, in order to avoid border effects that would artificially enlarge the value of the  $y_i$ -variance, the new variables

$$z_i = \cos(2\pi y_i), \quad i = 1, 2 \quad (13)$$

are introduced, and the diffusion measure  $D$  is computed on the  $(z_1, z_2)$ -space instead of on the actual action space  $(y_1, y_2)$ .

The range of the unperturbed integrals onto the  $(y_1, y_2)$ -plane for five bundles around the initial conditions listed in Table 1 is depicted in Fig. 6, but, as already stated, it wanders onto the  $(z_1, z_2)$ -plane, shown in Fig. 7, the one to be used to compute the coefficient  $D$  defined by (12). For each one of these figures, an ensemble of 100 initial conditions chosen at random in a neighborhood of size  $10^{-7}$  of conditions (i) to (v) were followed during  $10^7$  iterations of the map for both values of  $\epsilon_2$ .

Furthermore, the averaged value of the diffusion for each ensemble was computed after  $10^7$  iterations. The concomitant out-coming values of  $D$  are displayed in Table 2.

Let us note that the averaged values obtained for  $D$  fairly succeed in yielding a measure of the

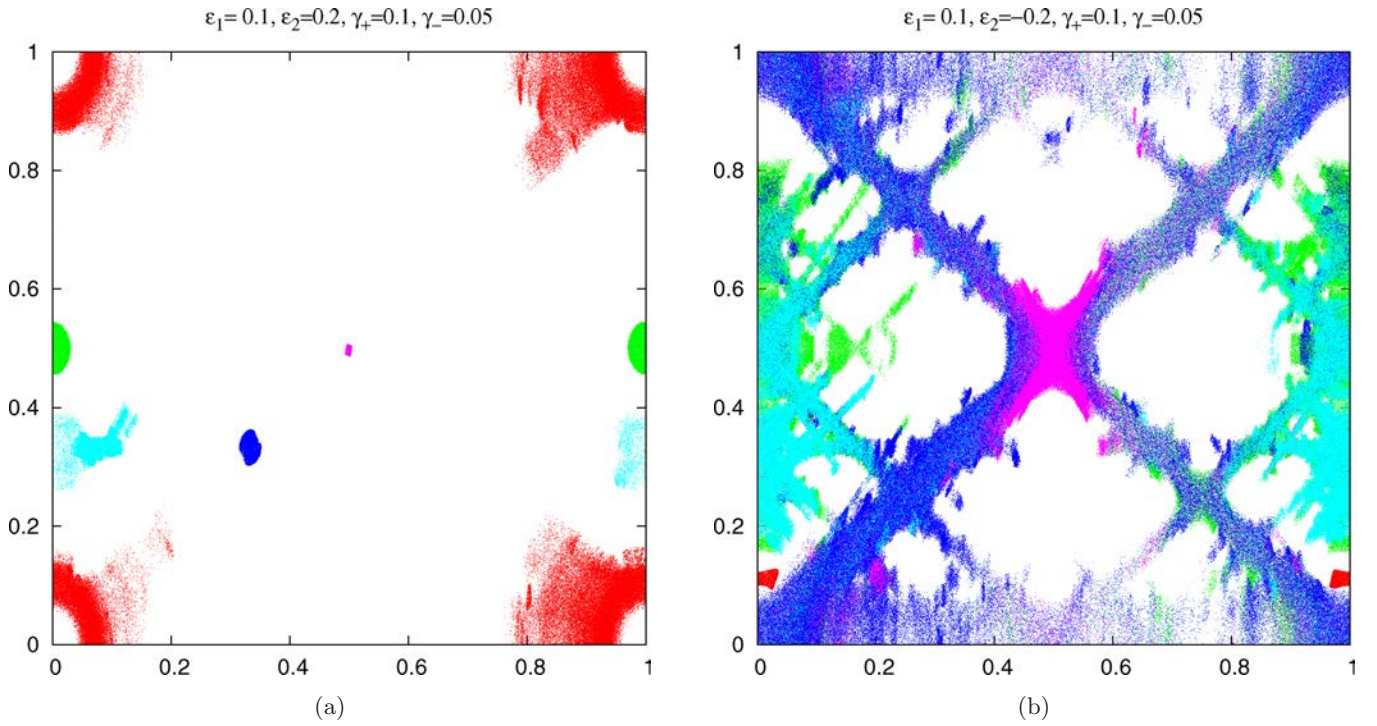


Fig. 6. Diffusion on action space after  $10^7$  iterations of the map for the bundles of 100 initial conditions chosen at random around initial conditions listed in Table 1. Initial condition (i) in red, (ii) in green, (iii) in blue, (iv) in purple and (v) in light-blue.

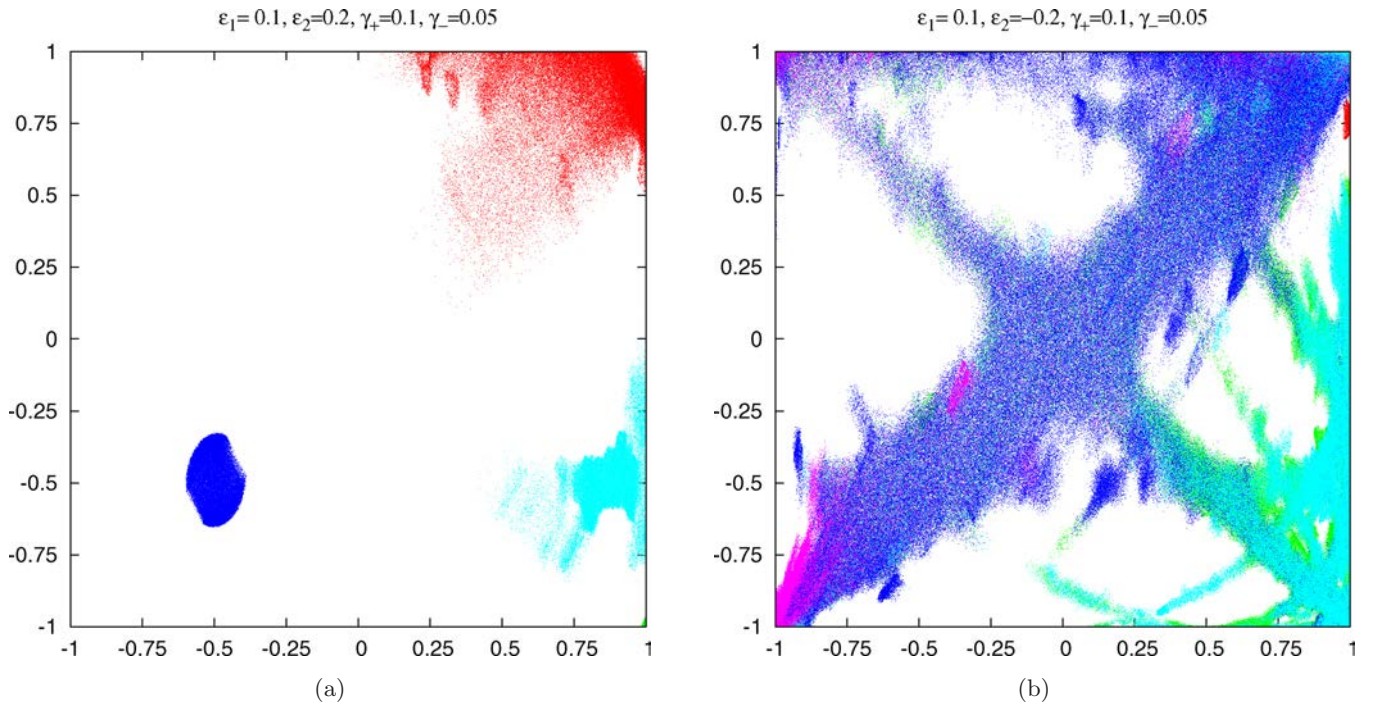


Fig. 7. Diffusion on  $(z_1, z_2)$ -space after  $10^7$  iterations of the map for the bundles of 100 initial conditions chosen at random around initial conditions listed in Table 1, using the same color scheme.

Table 2. Initial conditions on action space in units of  $2\pi/\epsilon_j, j = 1, 2$  (the same as in Fig. 1) for five different bundles of orbits and its concomitant value of  $\log(D)$  for  $\epsilon_2 = 0.2$  (fourth column) and  $\epsilon_2 = -0.2$  (last column).

| i.c.  | $y_1$ | $y_2$ | $\log(D)$          | $\log(D)$           |
|-------|-------|-------|--------------------|---------------------|
|       |       |       | $\epsilon_2 = 0.2$ | $\epsilon_2 = -0.2$ |
| (i)   | 0.000 | 0.110 | -8.666             | -10.145             |
| (ii)  | 0.000 | 0.500 | -11.093            | -7.438              |
| (iii) | 0.331 | 0.353 | -9.027             | -7.050              |
| (iv)  | 0.500 | 0.500 | -13.033            | -7.993              |
| (v)   | 0.074 | 0.336 | -9.512             | -8.034              |

domain covered by the wandering of each bundle of initial conditions, displayed in Fig. 7.

In fact, for  $\epsilon = 0.2$  the lowest value of  $D$  corresponds to regular orbits at (iv), whose range is practically restrained to a point where the motion is essentially stable. For the remaining initial conditions, the out-coming value of  $D$  is of the same order of magnitude, the unperturbed integrals remaining confined to rather small domains of comparable extent for the number of iterates considered.

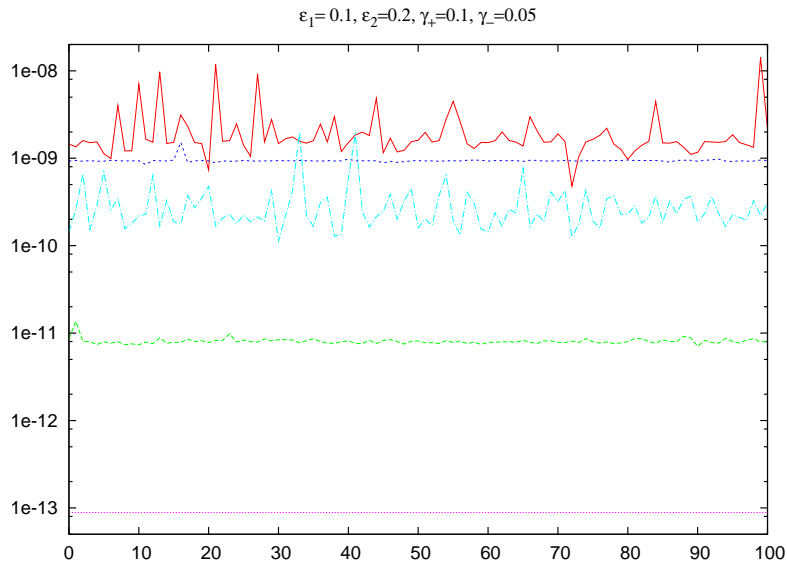


Fig. 8. Diffusion measure on action space after  $10^7$  iterations of the map for  $\epsilon_2 = 0.2$  for a random selection of 100 initial conditions around (i) in red, (ii) in green, (iii) in blue, (iv) in purple, and (v) in light-blue.

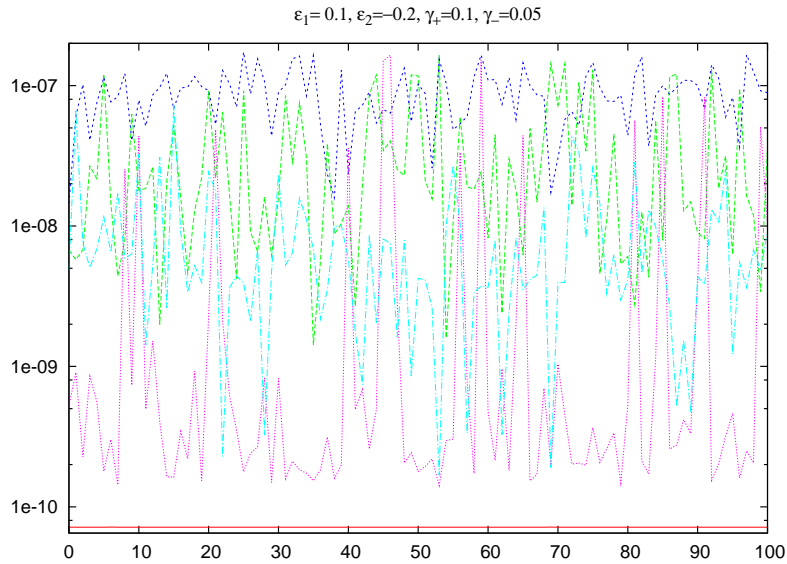


Fig. 9. Diffusion measure on action space after  $10^7$  iterations of the map for  $\epsilon_2 = -0.2$  for a random selection of 100 initial conditions around (i) to (v).

This fact can be confirmed when plotting the values of  $D$  for every orbit in each bundle as in Fig. 8, the last point in each curve corresponding to the averaged value for the ensemble.

The same procedure leads to Fig. 9 corresponding to  $\epsilon_2 = -0.2$ . In particular, this plot reveals the large dispersion in the values of  $D$  for each bundle, which gives account of the rather extended area swept by every bundle onto the  $(z_1, z_2)$ -plane.

Actually, it is not an easy task to cope with diffusion in multidimensional systems. Certainly, we could not invoke normal diffusion when dealing with systems of divided phase space. In fact, in such cases we ignore how the variance of the actions scale with time. Further, though theories on abnormal diffusion and subdiffusion or superdiffusion have been developed, they seem to apply only for low dimensional systems.

Thus, the computation of a diffusion coefficient reveals itself as a cumbersome task. For instance, in Fig. 9 we observe fluctuations of three orders of magnitude in the 100 values of  $D$  within a domain of  $10^{-7}$  around some of the chosen initial conditions.

Hence, in the forthcoming section we go beyond the search of an alternative tool to this end, bringing into play the finite time Shannon or Arnol'd Entropy and devote ourselves to determining its effectiveness for such an application.

## 6. The Shannon Entropy

Let us consider the time evolution of both normalized unperturbed actions  $(y_1\epsilon_1/2\pi, y_2\epsilon_2/2\pi)$  upon the torus  $T$ , or the unit square with opposite sides identified, as time goes on.

The evolution of the unperturbed integrals onto  $T$  is expected to be constrained to a small domain whenever a low diffusion takes place, while a large range should be in order in case of fast diffusion.

An adequate tool to measure diffusion is the finite time *Shannon Entropy*. (A theoretical background on Shannon Entropy can be found in e.g. [Shannon & Weaver, 1949; Katz, 1967; Arnol'd & Avez, 1989; Wehrl, 1978].)

Though in our opinion the Arnol'd formulation is more appropriate to formalize the mathematical framework, the Shannon approach is, perhaps, particularly suitable in order to provide a more intuitive understanding of the results. Thus, the main idea of the present approach is to make use of the Shannon Entropy, SE hereafter, in order to measure

the wandering of the unperturbed action variables when viewed on the unit square.

Following [Arnol'd & Avez, 1989], let us recall the definition of the function  $Z$  over  $[0, 1]$ :

$$Z(x) = -x \ln x, \quad x \in (0, 1]$$

$$Z(0) = 0,$$

which is continuous, non-negative and strictly concave ( $Z'' < 0$ ) and  $Z(x) = 0$  is equivalent to either  $x = 0$  or  $x = 1$ .

Further, let  $\alpha = \{a_i; i = 1, \dots, q\}$  be a partition of  $T$ , that is to say, a collection of  $q$  bidimensional boxes that cover the whole unit square. The boxes are assumed to be both measurable and disjoint, that is to say

$$\mu\left(T - \bigcup_i a_i\right) = 0, \quad \mu(a_i \cap a_j) = 0, \quad i \neq j,$$

where  $\mu$  stands for a measure and  $\bigcup_i a_i$  means the union of all the elements of the partition.

We can define a probability density on  $T$  by

$$\rho(x) = \frac{1}{N} \sum_{i=1}^N \delta(x - x_i), \quad (14)$$

where  $x_i$  denotes the result of a given iterate on  $T$ , and  $\delta$  is the *delta function*. It can be verified at once that

$$\int_T \rho(x) dx = 1, \quad (15)$$

and the probability of the element  $a_i$  of the partition turns out to be

$$\mu(a_i) = \int_{a_i} \rho(x) dx. \quad (16)$$

Finally, the entropy of the partition  $\alpha$  is defined as

$$S(\alpha) = \sum_{i=1}^q Z(\mu(a_i)) = - \sum_{i=1}^q \mu(a_i) \ln(\mu(a_i)). \quad (17)$$

Hence  $S(\alpha)$  is just the weighted logarithm of the number of elements in  $\alpha$ .

Let us note that for a given partition  $\alpha$ , the entropy is a bounded quantity. In fact, it is  $0 \leq S(\alpha) \leq \ln q$ . The minimum value is reached when all points fall in the very same element of the partition, say the  $k$ th element, which would correspond to the case of almost full stability (for instance, when all the iterates lie onto a single torus). Indeed, in such a case, we have a unique nonzero value  $\mu(a_k) = 1$ , yielding  $S = 0$ . On the other hand,

the maximum value,  $S(\alpha) = \ln q$ , will be reached whenever the  $q$  elements of the partition have equal measure  $\mu(a_i) = 1/q$ , that corresponds to the situation in which the unperturbed actions wander all over the unit square in a uniform fashion, i.e. in case of ergodicity.

Onwards,  $S$  will denote the normalized value of the entropy (i.e. the entropy divided by  $\ln q$ ) for a given partition  $\alpha$ .

Let us now accomplish the computation of the finite time SE for a given set of initial conditions for the CRSSM (4) with the same values of the set of parameters as those used in Sec. 3.

To this end, we take a partition of  $q = m \times m$  bidimensional boxes that cover the whole unit square, for an equi-spaced grid of  $400 \times 400$  and  $1000 \times 1000$  initial conditions in the domain  $(y_1 \epsilon_1 / 2\pi, y_2 \epsilon_2 / 2\pi) \in [0, 1) \times [0, 1)$ . The initial values for the remaining variables are  $x_1 = 0$ ,  $x_2 = 0$ .

The results after  $N = 10^5$  and  $10^7$  iterates of the map have been computed, with  $m = 100$  and  $m = 1000$ , respectively. Let us say that we have defined a partition in regards to the total number of

iterates such that in case of uniform distribution the same number of points would lie in each individual cell.

Let us mention that if we assume all the nonempty elements of the partition, say  $q_0$ , having the same measure, then  $S \approx \ln q_0 / \ln q$ . Therefore,  $q_0 \approx q^S$  so that  $(1 - S)$  will yield a measure of  $q_0/q$ .

The orbits with very small values of  $S$  lead to extremely slow diffusion, while those with large  $S$  correspond to very fast diffusion. Let us remark that in all the experiments performed, the results attained from the SE are also in quite good agreement with those obtained by recourse to the MEGNO, except in those regions of slow or fast diffusion. Thus, for making the comparison feasible, we have plot the values of the SE for a grid of  $1000 \times 1000$  initial conditions in the domain  $(y_1 \epsilon_1 / 2\pi, y_2 \epsilon_2 / 2\pi) \in [0, 1) \times [0, 1)$ , and after  $N = 10^7$  iterates of the map for the very same parameters used for the computation of the MEGNO. The results are given in Fig. 10, the plot on the left corresponding to  $\epsilon = 0.2$  and that on the right to  $\epsilon = -0.2$ .

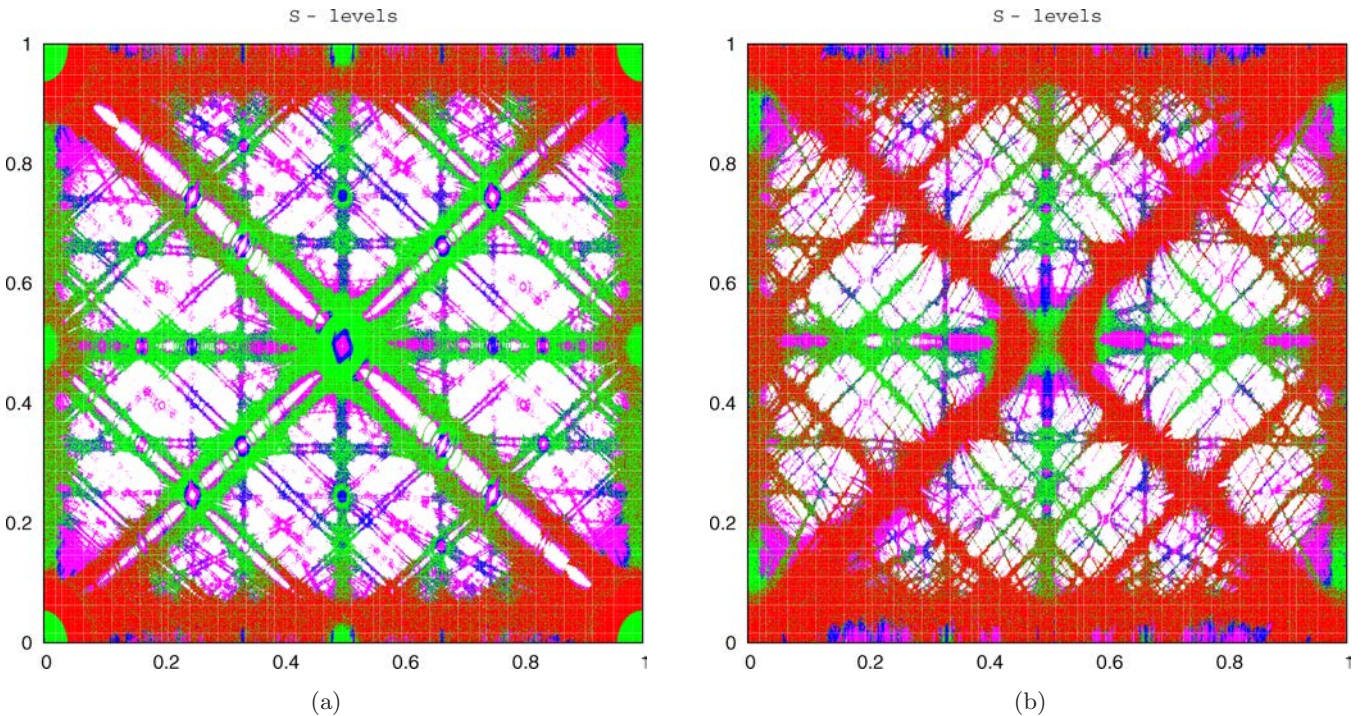


Fig. 10. S-levels for the CRSSM on the  $(y_1, y_2)$ -plane after  $N = 10^7$  iterates of the map for a grid of  $1000 \times 1000$  initial conditions of the unperturbed actions for  $\epsilon_2$  with opposite signs. Values of  $S < 0.38$  are depicted in white,  $0.38 \leq S < 0.45$  in purple,  $0.45 \leq S < 0.5$  in blue,  $0.5 \leq S < 0.66$  in green and  $0.66 \leq S$  in red. In terms of the number of visited elements of the partition,  $q_0$ , the intervals correspond to  $q_0 < 2 \times 10^2$  in white,  $2 \times 10^2 \leq q_0 < 5 \times 10^2$  in purple,  $5 \times 10^2 \leq q_0 < 10^3$  in blue,  $10^3 \leq q_0 < 10^4$  in green and  $10^4 \leq q_0$  in red.

Let us note that the resonance structure arising in the contour-plots obtained with the SE resembles the one revealed by the MEGNO. Moreover, the dramatic effect on the resonances due to the change of sign of  $\epsilon_2$  remains noticeable. Indeed, as already pointed out, in the case of positive  $\epsilon_2$  most of the resonances display an elliptical chain of tori at their center while for negative  $\epsilon_2$  several resonances show up as totally hyperbolic. However, while the MEGNO just measures the local hyperbolicity of a certain point in phase space, the SE provides information about chaotic diffusion at such a point. This can be clearly seen, for instance in the case for  $\epsilon_2 = -0.2$ , by the small values adopted by the SE along the resonance at  $y_2 = 0.5$ , whose structure seems to act as a barrier to diffusion as we have already shown.

Although the SE depends on the partition, in our experiments we have found no significant differences using different  $\alpha$ 's. Nonetheless, we observe a strong dependence of the SE values on the number of iterates as well as on the set of adopted initial conditions.

While for  $N \rightarrow \infty$  the SE (in phase space) should become the metric entropy, which is related to the sum of the positive Lyapunov's exponents, this seems not to be the case for any finite, though very large, number of iterates  $N$ .

## 7. Conclusions

The application of the generalized MEGNO to a multidimensional conservative map, the Coupled Rational Shifted Standard Map, succeeds in unveiling its global dynamical structure. The map turns out to be globally chaotic for the values of the parameters adopted in the numerical experiments herein, the chaotic component encompassing  $\sim 90\%$  of action space. In spite of this, hundreds of resonances can be clearly distinguished, presenting a chain of tori close to their centers that are elliptic for  $\epsilon_2 > 0$  and hyperbolic for  $\epsilon_2 < 0$ .

This solely fact seems to play a significant role in the efficiency of chaotic diffusion on action space. Indeed, as we have shown, though in both cases the action space is globally chaotic, the presence of resonances having either an elliptic or hyperbolic structure is determinant to allow fast diffusion.

The numerical evidence here presented reveals that only when the phase space has a dominant hyperbolic structure, diffusion may proceed through the relics of the unstable domain of resonances.

On the other hand, the elliptic structures of resonances, though chaotic, do not serve as routes to spread the stochastic motion, moreover they act as barriers to fast diffusion.

In any case, as we have already mentioned, the observed diffusion is not Arnol'd diffusion for which a globally chaotic phase space is certainly not a due scenario. Nevertheless, the results shown herein allows of being referred to as Arnol'd diffusion-like processes, at least accounting for their geometric resemblance.

On the other hand, even for extremely large motion times, the whole chaotic component seems not to be connected. Though this is still an open matter, the dynamical structure of multidimensional systems being so intricate make us assert that the chaotic component is not likely to be fully connected, at least in realistic physical systems like, for instance, the phase space corresponding to galaxies or asteroidal dynamical models.

Herein we have addressed the difficulties to compute a somewhat meaningful diffusion coefficient, due to the fact that, as far as we know, it still remains unclear which would be the due approach; in particular, how the variance of the variables scales with time other than in a random walk approximation in the case of multidimensional systems.

Moreover, a new tool has been proposed to attain a measure of change of the unperturbed actions, namely the finite time Shannon or Arnol'd Entropy. It contrives to provide a fairly accurate picture of the dynamics when compared with that yielded by the MEGNO, but with considerable some less computational effort. Indeed, it provides the global dynamical structure of the system and also measure diffusion with no need of computing the differential map, though larger time-scales are required. This fact becomes more important when dealing with Hamiltonian flows.

In a forthcoming paper we will discuss exhaustively the computation of the diffusion coefficient, considering normal (random walk) and anomalous diffusion, typical behavior near resonances (see e.g. [Zhou *et al.*, 2002; Cordeiro & Mendes de Souza, 2005; Cordeiro, 2006; Metzler & Klafter, 2000], as well as several particular aspects concerning the definition and computation of this coefficient).

Finally, we believe that much progress has to be done to understand the global instability properties of multidimensional systems.

## Acknowledgments

This work was supported with grants from the *Consejo de Investigaciones Científicas y Técnicas de la República Argentina*, and the *Universidad Nacional de La Plata*.

## References

- Arnol'd, V. I. [1964] “Instability of dynamical systems with many degrees of freedom,” *Sov. Math.-Dokl.* **5**, 581–586.
- Arnol'd, V. & Avez, A. [1989] *Ergodic Problems of Classical Mechanics*, 2nd edition (Addison-Wesley, NY).
- Cachucho, F., Cincotta, P. & Ferraz-Mello, S. [2010] “Chirikov diffusion in the asteroidal three-body resonance (5, 2, 2),” *CMDA* **108**, 35–58.
- Chirikov, B. V. [1979] “A universal instability of many-dimensional oscillator systems,” *Phys. Rep.* **52**, 263–379.
- Chirikov, B., Lieberman, M., Shepelyansky, D. & Vivaldi, F. [1984] “A theory of modulational diffusion,” *Physica D* **14**, 289–304.
- Chirikov, B. & Vecheslavov, V. [1989] “How fast is the Arnold diffusion?” *Novosibirsk* **89**, 1–94.
- Chirikov, B. & Vecheslavov, V. [1993] “Theory of fast Arnold diffusion in many-frequency systems,” *J. Stat. Phys.* **71**, 243–258.
- Cincotta, P. M. & Simó, C. [2000] “Simple tools to study global dynamics in non-axisymmetric galactic potentials — I,” *A&AS* **147**, 205–228.
- Cincotta, P. M. [2002] “Arnold diffusion: An overview through dynamical astronomy,” *New Astron. Rev.* **46**, 13–39.
- Cincotta, P. M. & Giordano, C. M. [2002] “Global dynamics through the mean exponential growth factor of nearby orbits (MEGNO),” *Proc. Advances in Space Dynamics 2. Applications in Astronomy*, eds. Winter, O. & Prado, A. F. B. A. (I.N.P.E., São Paulo), pp. 237–250.
- Cincotta, P. M., Giordano, C. M. & Simó, C. [2003] “Phase space structure of multi-dimensional systems by means of the mean exponential growth factor of nearby orbits,” *Physica D* **182**, 151–178.
- Cincotta, P. M. & Giordano, C. M. [2008] “Topics on diffusion in phase space of multidimensional Hamiltonian systems,” *New Nonlinear Phenomena Research*, ed. Perlidze, T. (Nova Science Publishers, NY), Chapter 6, pp. 393–410.
- Cordeiro, R. & Mendes de Souza, L. [2005] “Anomalous diffusion in the first-order Jovian resonance,” *A&A* **439**, 375–385.
- Cordeiro, R. [2006] “Anomalous diffusion in the Asteroid belt,” *AJ* **132**, 2114–2126.
- Gerhard, O. E. & Binney, J. J. [1985] “Triaxial galaxies containing massive black holes or central density cusps,” *MNRAS* **216**, 467–502.
- Giordano, C. M. & Cincotta, P. [2004] “Chaotic diffusion of orbits in systems with divided phase space,” *A&A* **423**, 745–753.
- Katz, A. [1967] *Principles of Statistical Mechanics, the Information Theory Approach* (W. H. Freeman & Co., San Francisco).
- Korabel, N. & Klages, R. [2004] “Fractality of deterministic diffusion in the nonhyperbolic climbing sine map,” *Physica D* **187**, 66–88.
- Lega, E., Guzzo, M. & Froeschlé, C. [2010] “A numerical study of the hyperbolic manifolds in a priori unstable systems. A comparison with Melnikov approximations,” *CMDA* **107**, 115–127.
- Lochak, P. [1999] *Proc. Hamiltonian Systems with Three or More Degrees of Freedom*, ed. Simó, C. (Kluwer, Dordrecht), pp. 168–183.
- Meiss, J. [1992] “Symplectic maps, variational principles, and transport,” *Rev. Mod. Phys.* **64**, 795–848.
- Merritt, D. & Friedman, T. [1996] “Triaxial galaxies with cusps,” *ApJ* **460**, 136–162.
- Merritt, D. & Valluri, M. [1996] “Chaos and mixing in triaxial stellar systems,” *ApJ* **471**, 82–105.
- Metzler, R. & Klafter, J. [2000] “The random walk’s guide to anomalous diffusion: A fractional dynamics approach,” *Phys. Rep.* **339**, 1–77.
- Milani, A. & Nobili, A. M. [1992] “An example of stable chaos in the Solar system,” *Nature* **357**, 569–571.
- Milani, A. [1993] “The Trojan asteroid belt: Proper elements, stability, chaos and families,” *CMDA* **57**, 59–94.
- Milani, A. & Farinella, P. [1994] “The age of the Veritas asteroid family deduced by chaotic chronology,” *Nature* **370**, 40–42.
- Milani, A., Nobili, A. M. & Knežević, Z. [1997] “Stable chaos in the asteroid belt,” *Icarus* **125**, 13–31.
- Morbidelli, A. & Froeschlé, C. [1996] “On the relationship between Lyapunov times and macroscopic instability times,” *CMDA* **63**, 227–239.
- Muzzio, J. C., Carpintero, D. D. & Wachlin, F. C. [2005] “Spatial structure of regular and chaotic orbits in a self-consistent triaxial stellar system,” *CMDA* **91**, 173–190.
- Papaphilippou, Y. & Laskar, J. [1998] “Global dynamics of triaxial galactic models through frequency map analysis,” *A&A* **329**, 451–481.
- Poincaré, H. [1893] *Les Méthodes Nouvelles de la Mécanique Céleste* (Gautier-Villars, Paris).
- Poon, M. & Merritt, D. [2002] “Triaxial black hole nuclei,” *ApJ* **568**, 89–92.

- Shannon, C. & Weaver, W. [1949] *The Mathematical Theory of Communication* (Illinois U. P., Urbana).
- Venegeroles, R. [2008] “Calculation of superdiffusion for the Chirikov–Taylor model,” *Phys. Rev. Lett.* **101**, 54102–54105.
- Wehrl, A. [1978] “General properties of entropy,” *Rev. Mod. Phys.* **50**, 221–260.
- Zhou, J., Sun, Y. & Zhou, L. [2002] “Evidence for Lévy random walks in the evolution of comets from the Oort cloud,” *CMDA* **84**, 409–427.